Chemical Engineering Journal xxx (xxxx) xxx–xxx

Contents lists available at ScienceDirect

Chemical Engineering Journal

journal homepage: www.elsevier.com/locate/cej

Study on transport phenomena and intrinsic kinetics for CO_2 adsorption in solid amine sorbent

M.J. Bos*, T. Kreuger, S.R.A. Kersten, D.W.F. Brilman*

Sustainable Process Technology, Faculty of Science and Technology, University of Twente, P.O. Box 217, 7500AE Enschede, Netherlands

HIGHLIGHTS

- New method to measure intrinsic CO_2 adsorption kinetics for amine sorbents.
- Adsorption kinetics measured for Lewatit VP OC 1065 sorbent.
- Linear driving force not able to describe effect CO_2 pressure.
- Toth isotherm based rate equation successfully describes CO_2 adsorption kinetics.

ARTICLE INFO

Keywords:
Intrinsic adsorption kinetics
CO_2 capture
Supported amine sorbent
Lewatit VP OC 1065

ABSTRACT

A study on the intrinsic kinetics of CO_2 adsorption on solid amine sorbent is performed. For this, a new experimental method is developed to exclude heat and mass transfer limitations during the kinetic adsorption experiments. Hereto a novel contactor was designed and good process control, working with pure CO_2 and small particle diameters enabled the measurement of intrinsic kinetics. A mathematical model describing convection, diffusion and reaction rate inside a particle confirmed the absence of mass and heat transfer limitations in the experiments. Linear driving force and Toth-isotherm reaction rate equations are evaluated for the CO_2 adsorption process studied. The results show that the experimental particle loading with time could not be described by the linear driving force models. On the other hand, the Toth reaction rate equation, consistent with the Toth isotherm to describe the adsorption equilibrium, showed a very good fit to the experimental data. This shows that a rate based isotherm equation is necessary for prediction of both adsorption rate and equilibrium loading. It also implies that there is a strong correlation between the kinetic rate parameters found and the adsorption equilibrium parameters used, which was confirmed in this study.

1. Introduction

Because of anthropogenic emissions of CO_2 the concentration in the atmosphere is increased from 250 ppm in pre-industrial area to more than 400 ppm nowadays [1]. Air capture is needed to lower the concentrations [2] and might even be necessary to meet the Parisian climate goals [3,4]. Additionally, air capture of CO_2 opens the opportunity of producing renewable fuels at locations with excess renewable electricity but without point sources of CO_2. For example, methanol can excellently be produced from CO_2 and renewable H_2 [5–7]. Alternatively, air captured CO_2 can be used in green houses to raise CO_2 concentrations or for algae cultivation [8].

Choi et al. [9] published an overview of the properties of multiple solid sorbents for CO_2 capture. It was shown that solid amine sorbents are excellent CO_2 capture compounds because of high capacities at low partial pressure of CO_2 and low regeneration temperature ($<100\,°C$) [9].The advantages of solid amine sorbents versus liquid amine solvents for CO_2 capture are given by Shakerian [10]. Ünveren et al. [11] reviewed the mechanism and capacity of CO_2 adsorption on different solid amine sorbents.

The solid amine sorbent used in this study is Lewatit VP OC 1065, which is polystyrene spherical sorbent with a benzylamine functional group. In literature Lewatit VP OC 1065 is shown to be an effective sorbent for flue gas CO_2 capture [12], CO_2 capture from biogas [13,14], deep removal of sour gases from natural gas [15] and air capture of CO_2 [16].

For adsorption of CO_2 in aqueous amine systems two reaction mechanisms are commonly assumed. That is, the zwitterion mechanism initially proposed by Caplow [17] and the termolecular mechanism initially proposed by Crooks and Donnellan [18]. In the termolecular

* Corresponding authors.
E-mail addresses: martin.bos@utwente.nl (M.J. Bos), wim.brilman@utwente.nl (D.W.F. Brilman).

https://doi.org/10.1016/j.cej.2018.11.072
Received 12 June 2018; Received in revised form 8 November 2018; Accepted 10 November 2018

mechanism it is assumed that the amine bonding to CO_2 and the proton transfer from the amine to an additional base is simultaneously. Whereas, in the zwitterion mechanism this process is assumed to be a two step process with the zwitterion as an intermediate. In aqueous systems the additional base can either be a H_2O molecule or an amine group. More details about the reaction mechanisms of aqueous benzylamine can be found in publications of Mukherjee et al. [19] and Richner et al. [20]. Mukherjee et al. [19] concluded that the termolecular mechanism is more likely than the zwitterion mechanism based on interpretation of experimental results of CO_2 absorption in aqueous benzylamine.

In absence of H_2O during CO_2 adsorption on solid amine sorbent the only available base for reaction is another amine group. Therefore two amine groups should be in close proximity to adsorb one molecule of CO_2. Molecular modelling of Lewatit VP OC 1065 by Buijs and de Flart [21] showed that the amine groups alternate in position and are in close vicinity of each other. This shows that two amine groups could react with each other despite being fixated on the surface. DFT calculations by Buijs and de Flart indicated that the either the H_2O catalyzed (in humid conditions) or the amine catalyzed (in dry conditions) formation of a carbamic acid is the most likely reaction mechanism.

Membane et al. [22] showed the importance of diffusive intermediates in the CO_2 adsorption in PEI on silica. Hypothesised was the mobility of zwitterions, however DFT calculations questioned the stability of zwitterions in dry conditions. For the adsorption of CO_2 on amines on SBA-15 Hahn et al. [23] showed the formation of carbamate using in situ FTIR. In the presence of H_2O the carbamate was found to be more stable. Yu et al. [24] found the formation of carbamate for primary amines while carbamic acid was formed for secondary amines. Again H_2O was found to stabilize the products. Bacsik et al. [25] showed formation of both carbamate and carbamic acid using insitu FTIR for propylamines on silica. Literature seems to have reached consensus that carbamate is formed with primary amines on solid sorbent. The exact mechanism however remains unclear, although DFT calculations question the formation of zwitterions. Therefore, the formation by a termolecular mechanism seems more likely.

Analysing kinetics of adsorption is important for reactor sizing and process optimization. Commonly, kinetics of adsorption are determined in fixed bed experiments [26–29] or in TGA apparatus [30–35]. However, in fixed bed adsorption experiments isothermal plug flow conditions are almost never achieved. Therefore, significant numerical modelling [26] has to be applied to determine kinetics from fixed bed operation and account for dispersion and temperature increases. In TGA, supply limitations might be present due to low gas flow rates and isothermal operation is challenging. Therefore, to determine intrinsic kinetics more accurate experiments have to be performed. For example, in a spinning basket reactor [36] or a differential fixed bed [37].

This paper describes an new experimental method to measure intrinsic kinetics of CO_2 adsorption on solid amine sorbents. In this method an flat bed reactor is used in combination with the supply of pure CO_2 to the sorbent. Thereby, mass transfer and supply limitations potentially are eliminated and good heat transfer is achieved by direct contact of the sorbent with the temperature controlled bottom plate. Validation of the new experimental method is discussed. Next to the new experimental method, results for the intrinsic kinetics of Lewatit VP OC 1065 are shown. This is one of the few studies were intrinsic kinetics – totally in absence of transport limitations – of CO_2 adsorption on solid amine sorbents are discussed.

2. Materials and methods

2.1. Materials

The solid amine sorbent studied in this work is Lewatit VP OC 1065 supplied by Lanxess. Lewatit VP OC 1065 has a primary benzylamine group that reacts with CO_2 [38]. The benzylamine group is supported on a polystyrene backbone crosslinked with divinylbenzene. The sorbent is shipped as spherical particles with an average diameter of 520 µm. The surface area, pore volume and pore diameter are 50 $m^2 g^{-1}$, 0.27 $cm^3\ g^{-1}$ and 25 nm respectively [39]. The CO_2 gas used is supplied by Praxair, the Netherlands in 99.9993% purity. More material properties, model symbols and abbreviations can be found in Table 1.

Table 1
Material properties and model symbols.

Symbol	Value	Unit	Meaning	Reference
b		bar^{-1}	Toth isotherm equilibrium parameter	
C		mol m_g^{-3}	Gas concentration	
C_{p,CO_2}	0.85	kJ kg_g^{-1}	CO_2 heat capacity	[40]
$C_{p,s}$	1.58	kJ kg_s^{-1}	Sorbent heat capacity	[14]
D		$m_g^2\ s^{-1}$	Diffusion coefficient	
d_s	0.2	mm	Particle diameter	
k			Kinetic constant	
M	0.044	kg mol^{-1}	Molar mass CO_2	[40]
n		mole	Number of moles	
NSD			Normalised standard deviation	
P			Pressure	
q		mol kg_s^{-1}	Particle loading	
q_e		mol kg_s^{-1}	Equilibrium loading at present conditions	
q_s		mol kg_s^{-1}	Absolute maximum particle loading	
R	8.314	J $mole^{-1}\ K^{-1}$	Gas Constant	
R_{ads}		mol $kg_s^{-1}\ s^{-1}$	Adsorption rate	
r_{pore}	12.5	nm	Pore radius	[39]
r		m	particle radius	
SSE			Sum of squared errors	
t		s	time	
t_h			Toth isotherm heterogeneity parameter	
T		K	Temperature	
V		K	Volume	
			Greek Symbols	
χ			Toth isotherm parameter	
$\Delta_r H$	75	kJ mol^{-1}	Reaction heat	[14]
ε	0.23	$m_{pore}^3\ m_s^{-3}$	Particle voidage	[39]
λ_{CO_2}	0.016	W $m^{-1}K^{-1}$	CO_2 thermal conductivity (1 bar, 293 K)	[40]
λ_s	0.43	W $m^{-1}\ K^{-1}$	Sorbent thermal conductivity	Section 2.7
μ_{CO_2}	$1.5{\cdot}10^{-5}$	Pa s^{-1}	CO_2 viscosity (1 bar, 293 K)	[40]
ρ_s	880	kg m_s^{-3}	Sorbent density	[12]
ρ_{CO_2}	1.8	kg m_g^{-3}	CO_2 density (1 bar, 293 K)	[40]
τ	2.3	$m_g\ m_s^{-1}$	Pore tortuosity	[12]
			Subscripts	
ads			Adsorption	
des			Desorption	
g			Gas	
LDF1			Pseudo-first order Linear Driving Force	
LDF2			Pseudo-second order Linear Driving Force	
p			Pore	
s			Sorbent	
Toth			Toth isotherm	

2.2. Experimental Setup

About 1.35 gram of sorbent is loaded in a flat bed reactor (see Fig. 1) of 150 mm diameter and 10 mm height constructed of stainless steel. A thin layer of sorbent – close to monolayer – is in contact with the thermostated bottom plate of the reactor. The thin layer of sorbent is covered with a 5 µm wire mesh topped with 1 mm diameter stainless

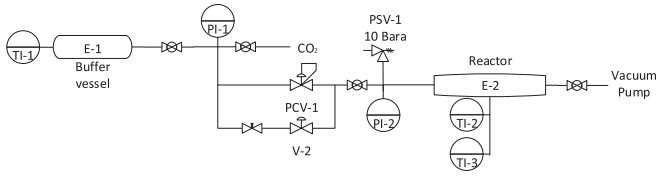

Fig. 1. Experimental set-up to measure adsorption kinetics.

steel spheres to fixate the layer of sorbent. Initially, the sorbent is cleaned from H_2O and CO_2 by heating to 80 °C (Julabo 6-MW) and reducing the absolute pressure to less than 1 mbar in the reactor by a vacuum pump (Edwards E2M2). After cooling (Julabo F12-MW) the reactor to experimental temperature, Grade 5.3 CO_2 (Praxair) is fed from the supply vessel (E-1, Fig. 1)) to the headspace in the reactor (E-2, Fig. 1) through the inlet in the cylindrical wall.

Pressure in the reactor and supply vessel is monitored by high precision pressure sensors (Heise DXD ± 0.02% full scale, PI-1: 0-30 PSI, PI-2: 0-20 PSI). The pressure inside the reactor is controlled by a pressure controller (PCV-1, Fig. 1, Brooks 5866 series). Because the response of the pressure control valve is slow compared to adsorption kinetics a bypass solenoid valve (V-2, Fig. 1) is installed to instantaneously increase the reactor pressure to the experimental pressure. The opening of the valves and data acquisition is performed using Labview. The bypass valve is opened for a few hundred milliseconds after which it is automatically closed. Flow through V-2 can be restricted by a needle valve. Temperature is monitored using PT-100 temperature sensors. Temperature is monitored in the buffer vessel (TI-1, Fig. 1) and two radial positions inside the reactor (TI-2 and TI-3, Fig. 1).

2.3. Experimental and interpretation methods

An experimental cycle consist of three steps: regeneration, cooling and experiment. The same batch of sorbent is reused for all experiments. Regeneration is performed at 80 °C and vacuum pressure (< 1 mbar) to clean the sorbent from CO_2. Before the first experiment of a sorbent batch the sorbent is cleaned from water and CO_2 by heating to 80 °C and purging nitrogen overnight. After 1.5 h of regeneration, cooling to the experimental temperature is performed under vacuum pressure. At the start of the experiment, the reactor is at experimental temperature and vacuum pressure (< 1 mbar). The supply vessel has a pressure of approximately 2 bar of pure CO_2 and is at room temperature at the start of the experiment. Next, the pressure control valve and bypass valve are opened in parallel (defined as $t = 0$). From this point on the experiment is performed at isothermal and isobaric (after reaching the experimental pressure) conditions. Experiments have been performed at 50/100/200 mbar and in the temperature range of 5–40 °C.

Using the pressure and temperature in the supply vessel and the reactor the number of moles of CO_2 on the sorbent can be calculated using Eq. (1) In this equation the (small) volume of the pipelines upstream and downstream the valves is clubbed with respectively the value for the buffer vessel volume or the reactor volume. The compressibility factor of CO_2 is not taken into account because the maximum pressure is 2.5 bara, which means the compressibility factor is higher than 0.99 [41]. Following, the sorbent loading can be calculated from Eq. (2) where $m_{\text{sorbent,wet}}$ [kg] is the wet sorbent mass as weighted and $\text{MC}_{\text{sorbent}}$ the moisture content on the stock sorbent, see Table 3.

$$n_{CO_2,\text{ads}}(t) = \left[\frac{P_{\text{reac}}V_{\text{reac}}}{RT_{\text{reac}}} + \frac{P_{\text{buf}}V_{\text{buf}}}{RT_{\text{buf}}}\right]_{t=0} - \left[\frac{P_{\text{reac}}V_{\text{reac}}}{RT_{\text{reac}}} + \frac{P_{\text{buf}}V_{\text{buf}}}{RT_{\text{buf}}}\right]_{t=t} \tag{1}$$

$$q(t) = \frac{n_{CO_2,\text{ads}}(t)}{m_{\text{sorbent,wet}}\cdot(1 - \text{MC}_{\text{sorbent}})} \tag{2}$$

From the sorbent loading the adsorption kinetic constant (k_{ads}) is found by fitting the integrated rate equation (see Section 2.4) on the experimental loading versus time curve. The rate equation is integrated either manually for the linear driving rate force equations or numerically using the ode45 function in Matlab for the Toth rate equation. Fitting of the loading curve is performed by the least-square fit function lsqcurvefit in matlab.

2.4. Reaction rate equation

In this study we evaluate the sorption kinetics of CO_2 on a solid amine sorbent, aiming to identify the intrinsic reaction kinetics in absence of mass transfer limitations. In the evaluation multiple kinetic rate equations are used. Below, the equations used are shortly summarized:

- **Pseudo-first order** linear driving force model: The most simple and straight forward model and therefore often used in literature. The linear driving force (LDF) definition by Glueckauf [42] is used and not the often used Lagergren [43] pseudo first order definition. Differences in both interpretations are discussed by Rodrigues and Silva [44].

$$\frac{\partial q}{\partial t} = k_{\text{LDF1}}P_{CO_2}(q_e - q) \tag{3}$$

  In this equation k_{LDF1} is the kinetic constant, P_{CO_2} is the CO_2 (partial) pressure in the reactor, q_e the equilibrium loading at the corresponding CO_2 (partial) pressure and temperature in the reactor and q the loading at time t. q_e is determined by the Toth isotherm, see Table 2. The gas concentration is included in the form of the CO_2 pressure because Veneman et al. [12] showed the necessity.
- **Pseudo-second order** linear driving force model: Because in dry conditions two amine molecules are needed to capture one CO_2 molecule, the pseudo-second order is more correct from a mechanistic point of view.

$$\frac{\partial q}{\partial t} = k_{\text{LDF2}}P_{CO_2}(q_e - q)^2 \tag{4}$$

  Again k_{LDF2} is the kinetic constant, P_{CO_2} is the CO_2 pressure, q_e and q the loading at equilibrium with the reactor conditions and at time t respectively.
- **Toth** rate equation: The Toth isotherm is a Langmuir-based isotherm modified with a surface heterogeneity parameter t_h, see Table 2. Consequently, this parameter is found in the rate equation [45].

$$\frac{\partial q}{\partial t} = k_{\text{Toth}}\left\{P_{CO_2}\left[1 - \left(\frac{q}{q_s}\right)^{th}\right]^{\frac{1}{t_h}} - \frac{1}{b}\frac{q}{q_s}\right\} \tag{5}$$

  In this equation k_{Toth} is the kinetic constant, P_{CO_2} is the CO_2 pressure in the reactor, q_s is the maximum loading of CO_2 on the sorbent at any conditions, b is the equilibrium parameter which is also defined as $b = \frac{k_{ads}}{k_{des}}$ and q is the loading at time t. The parameters q_s, t_h and b can be determined by fitting the equilibrium capacities on the isotherm, see Section 3.1 and Tables 2 and 4.

Table 2
Toth isotherm equations.

$q_e = \frac{q_s bP_{CO_2}}{(1+(bP_{CO_2})^{th})^{1/t_h}}$	(1)
$b = b_0 \cdot exp\left(\frac{\Delta H_0}{RT_0}\left(\frac{T_0}{T} - 1\right)\right)$	(2)
$t_h = t_{h0} \cdot \alpha\left(1 - \frac{T_0}{T}\right)$	(3)
$q_s = q_{s0} \cdot exp\left(\chi\left(1 - \frac{T}{T_0}\right)\right)$	(4)

Table 3
Error in parameters. The column 'standard deviation' shows the value of two standard deviations (95% confidence intervals) from the experiments. The column 'error' shows either the error by accuracy of the device or the error by propagation of errors for calculated values.

Parameter	Symbol	Value	Standard deviation	Error	Unit
Moisture content sorbent	$MC_{sorbent}$	0.449	0.016	–	$kg_{moisture} \cdot kg^{-1}_{sorbent}$
Pressure Reactor	P_{reac}	$1.4 \cdot 10^5$		28	Pa
Pressure Buffer vessel	P_{buf}	$2.1 \cdot 10^5$		41	Pa
Temperature	T_i			0.5	*K*
Volume Buffer vessel	V_{buf}	114.4	1.2	0.7	mL
Volume Reactor	V_{reac}	160.2	1.3	1.1	mL
Volume calibration vessel	V_{cal}	516.6	1.2	–	mL
Wet mass sorbent	$m_{sorbent,wet}$	1.35		0.01	g

To determine the accuracy of fitted rate constants the Sum of Squared Errors of prediction (SSE) was calculated. For the fit of k_{ads} on the loading versus time curve this can be done with Eq. (6).

$$SSE = \sum (q(t)_{exp} - q(t)_{mod})^2 \quad (6)$$

In this equations is $q(t)_{exp}$ the experimental measured loading at time t and $q(t)_{mod}$ the loading predicted by the rate equation. To determine the SSE for the Arrhenius plot the $q(t)_{exp}$ and $q(t)_{mod}$ are replaced by k_{exp} and $k_{Arrhenius}$.

2.5. Error analysis and reproducibility

Error analysis have been performed on the experimental determined loading. The method of propagation of errors is used [46]. In Section 1 of the Supporting Information more details about the calculations can be found. In Table 3 the parameters and their errors are shown. The error of pressure sensors have been checked by calibration using a dead weight tester (Tradinco T2400-1) in the pressure range above atmospheric pressure and a pressure calibrator (Beamax MC-5) in the reduced pressure range. The errors found after calibration are within sensor accuracy. The PT-100 temperature sensors have been checked using a water bath and a analogue mercury temperature indicator.

The buffer vessel and reactor volumes have been determined using a separate calibration vessel (V_{cal}) and equilibration of nitrogen pressure. Using the pressure before and after equilibration the unknown volume can be determined. The volume of the calibration vessel is determined by filling it with water and measure the mass increase. The error shown for the calibration vessel in Table 3 is the standard deviation (95% confidence interval) of four measurements. The error shown for the reactor and buffer vessel is either the standard deviation of four measurements (column standard deviation, Table 3) or the error by propagation of the error in the pressure and calibration vessel (column error, Table 3). The value of the standard deviation has been used in further error propagation calculations.

The moisture content of the sorbent has been determined using TGA apparatus (Netsch STA-449). The average value and standard deviation of four measurements are shown in Table 3. The wet sorbent mass added to the reactor has been determined using an analytic balance (Mettler AE100).

The error found in the loading is $\pm$ 0.19 mol kg^{-1} which is a significant relative error at low sorbent loading, although the relative error goes down rapidly with increasing sorbent loading. However, the reproducibility of the data seems to be much larger than $\pm$ 0.19 mol kg^{-1} as is shown in Fig. 2. It is seen that the maximum difference between a duplicate measurement is 0.02 mol kg^{-1} for the fast experiment (30 °C & 200 mbar) and 0.03 mol kg^{-1} for a triplet measurement of a slow experiment (5 °C & 100 mbar). More duplicate experiments are shown in Section 4.1.

2.6. Particle model

A mathematical model for diffusion and reaction into a spherical particle is constructed to verify the absence of mass and heat transport limitations in the experimental dataset.

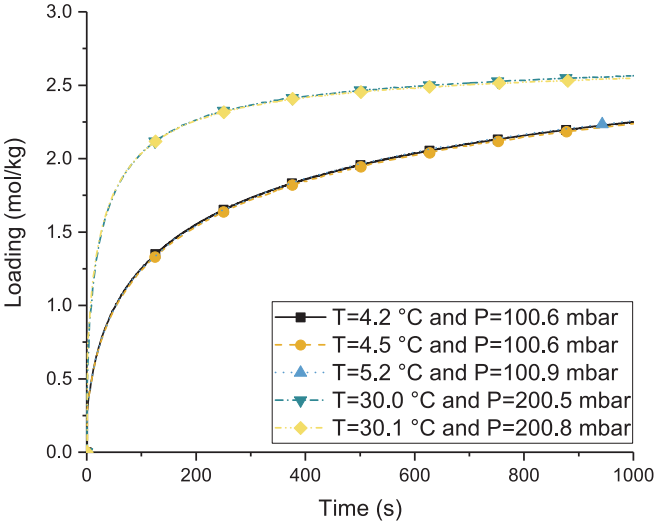

Fig. 2. Examples of reproducibility of a slow (5 °C & 100 mbar) and a fast (30 °C & 200 mbar) experiment. Symbols are added to increase distinction between lines.

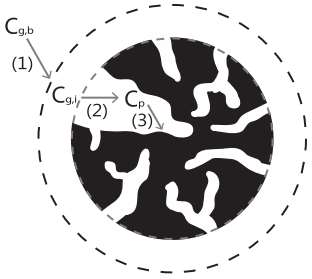

Fig. 3. Schematic overview of transport phenomena during CO_2 adsorption into a particle. $C_{g,b}$ is the gas bulk concentration, $C_{g,i}$ the gas interface concentration on the particle outer surface and C_p the gas concentration inside the particle pores. (1) shows the film layer resistance, (2) the diffusional transport into the pores and (3) reaction with the amine on the solid surface.

During adsorption of CO_2 on porous solid sorbents three stages of mass transfer can be distinguished as shown in Fig. 3. First, CO_2 has to be transported from the bulk through the film layer resistance to the interface (1, Fig. 3), also referenced to as external mass transfer. Next, CO_2 has to be transported into the pores of the particle (2, Fig. 3) as only little CO_2 can adsorb on the outer surface of the particle. This internal mass transfer is normally limited by either molecular or knudsen diffusion [47]. In case of a total pressure difference inside the pores viscous flow can play a role [47]. Finally, the CO_2 can react with the amine groups on the surface (3, Fig. 3). Transport phenomena for

heat transfer are analogue, as internal transfer by conduction through the particle plays a role and external transport by convection or conduction into the surrounding gas or the reactor wall as well.

In Eq. (7) the gas phase balance can be seen. The variables used in the equations below can be found in Table 1. For transport into the pores Knudsen diffusion and viscous flow [47] are included.

$$\varepsilon\frac{\partial C}{\partial t} = \frac{1}{r^2}\frac{\partial}{\partial r}\left[r^2\frac{\varepsilon}{\tau}\left(\frac{4}{3}\frac{r_{\text{pore}}}{2}\sqrt{\frac{8RT}{\pi M}} + \frac{r_{\text{pore}}^2}{8\mu}CRT\right)\frac{\partial C}{\partial r}\right] - \rho_s R_{\text{ad}} \tag{7}$$

The solid phase balance is shown in Eq. (8)and R_{ad} is defined by the rate equations shown in Eqs. (3)–(5).

$$\frac{\partial q}{\partial t} = R_{\text{ad}} \tag{8}$$

The energy balance is shown in Eq. (9) and used to determine temperature profiles inside the particle.

$$\rho_s C_{p,s}\frac{\partial T}{\partial t} = \frac{1}{r^2}\frac{\partial}{\partial r}\left[r^2\lambda_s\frac{\partial T}{\partial r}\right] + \Delta_r H\rho_s R_{\text{ad}} \tag{9}$$

2.7. Thermal conductivity

The thermal conductivity of the sorbent particle was found to be an important parameter to predict if significant temperature gradients exist within in a particle. However, no literature data was found for Lewatit VP OC 1065 or polystyrene particles. Therefore, it was decided to measure the thermal conductivity of the sorbent. The thermal conductivity of the sorbent is determined by investigating temperature gradients within a fixed bed of particles, heated from the cylindrical wall and bottom area. From these experiments the effective thermal conductivity through the sorbent/air bulk can be determined. With the equation by Zehner and Schlünder [48] the measured effective thermal conductivity can be translated into the solid thermal conductivity. An average value of 0.43 W m^{-1} K^{-1} was found for the solid thermal conductivity. More details about the experimental methods and calculations can be found in the Section 2 of the Supporting Information.

3. Validation of the experimental method

3.1. Equilibrium capacity

The equilibrium capacity is an important factor in the rate equations as shown in the Section 2.4. From literature [49,13–15] it is known that the Toth isotherm fits the equilibrium capacity well. However, in the study of Veneman et al. only a relatively small temperature range (303–373 K) is validated. In order to validate the kinetic rate equation in a larger temperature range new isotherm parameters are fitted. The experimental equilibrium data of Veneman et al. [49] is used. Additionally, equilibrium data from Sutanto et al. [13] is taken to include high temperature data. In this study, additional low temperature (278 K & 288 K) equilibrium capacities are measured. To check the experimental method used in this study equilibrium capacities are measured at 313 K and compared to data measured by Veneman et al. The found equilibrium capacities correspond well with capacities by Veneman et al. In Fig. 4 an overview of the data points is given.

The data have been fitted using least square minimization by the Globalsearch function in Matlab. The Normalized Standard Deviation (NSD) have been calculated with Eq. (10). In this equation q_{exp} is the experimental measured equilibrium capacity and $q_{isotherm}$ the loading predicted by the isotherm. N is the number of experimental points.

$$NSD(\%) = \sqrt{\frac{\sum[(q_{exp} - q_{isotherm})/q_{exp}]^2}{N-1}} \times 100 \tag{10}$$

The parameters found are shown in Table 4 and compared with the Veneman parameters. It should be noted that the maximum capacity q_{s0} is fixed to 3.4 mol kg^{-1} for two reasons. First, the nitrogen loading in the sorbent is 6.8 mol kg^{-1} [50] and two amine molecules are needed to capture one CO_2 molecule in dry conditions. Second, it was seen that the fixation of q_{s0} significantly reduced the NSD. Next to fitting the data to the Toth isotherm it was tried to fit the Langmuir isotherm in order to reduce fitting parameters on both the isotherm and rate equation. However, opposite to results by Sonnleitner et al. [14] no accurate fit could be found.

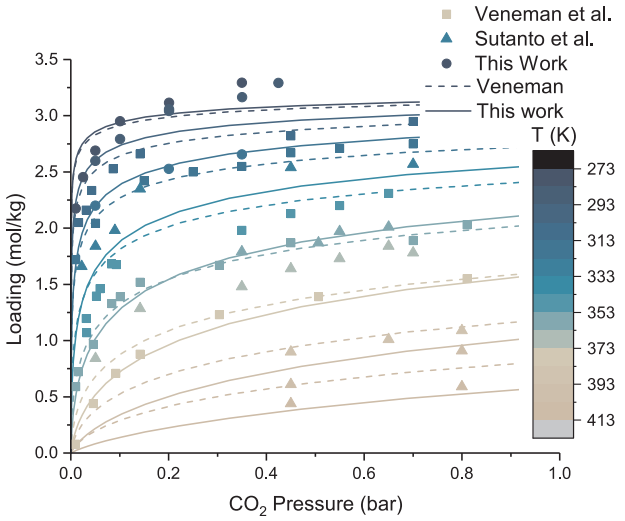

Fig. 4. Experimental equilibrium capacity (symbols) determined by Veneman [49] (squares), Sutanto [13] (triangles) and this work (rounds). The lines represent the Toth isotherm fitted in this work (lines) and by Veneman (stripes) as comparison. The lines plotted range from 273 K to 413 K with 20 K intervals.

Table 4
Isotherm parameters.

Symbol	Veneman et al. [49]	This work	Unit
	Parameter set A	Parameter set B	
q_{s0}	3.40	3.40	mol kg^{-1}
χ	0	0	–
T_0	353.15	353.15	K
b_0	408.84	93.0	bar^{-1}
ΔH_0	86.7	95.3	kJ mol^{-1}
t_{h0}	0.30	0.37	–
α	0.14	0.33	–
NSD	15.4	7.7	%

As is shown in Table 4 the NSD on the data set presented in Fig. 4 for the Veneman isotherm is significantly larger than for the fit in this work. In Fig. 5A can be seen that the Veneman isotherm significantly deviates from the parity plot outside the original temperature range. That is, at higher (> 100 °C) and lower (< 30 °C) temperatures. This means that the average accuracy of the isotherm reduces from ± 0.09 mol kg^{-1} originally to ± 0.15 mol kg^{-1} on the dataset presented here. Furthermore, it is seen that both isotherms are under predicting the capacity at temperatures below 20 °C. This might be an effect of change in mechanism as the absolute maximum (3.4 mol kg^{-1}) of one CO_2 molecules reacting with two amine groups is approached. Additionally, it is shown in Fig. 5B that the isotherm presented here is accurate in range from 20 to 140 °C resulting in an average accuracy of ± 0.12 mol kg^{-1} over the whole temperature range.

3.2. Effect of bypass valve V-2

During initial screening experiments it was found that the adsorption rate is fast. As a result, the initial pressure increase from vacuum to

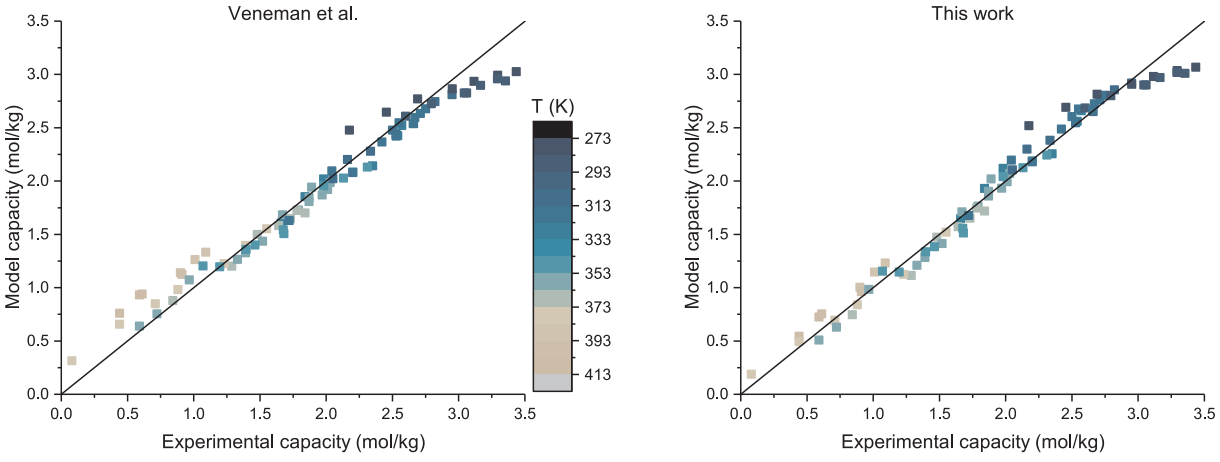

Fig. 5. Parity plot for the Toth isotherms presented in Table 4. The temperature colour map is shared between the figures.

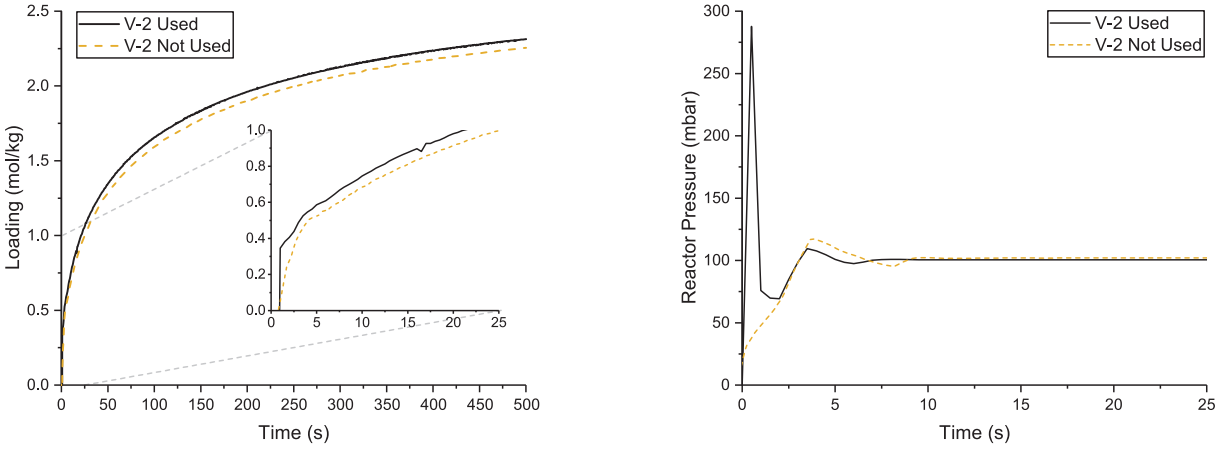

Fig. 6. Effect of the bypass valve V-2 on the initial reaction rate at 20 °C and 100 mbar of pure CO_2 for particles with a diameter between 150 and 250 µm.

the experimental pressure was found to be relatively slow. As shown in Fig. 6B the pressure increase takes about 5 s to reach the experimental pressure for the 100 mbar experiment. This might have two consequences. First, the reactor pressure is not constant in the initial phase of the adsorption process. However, this is the most optimal phase to determine adsorption kinetics since the influence of equilibrium is minimal. As seen in Fig. 6A the sorbent loading is already as high as 0.5 mol kg^{-1} after 5 s which is around 20% of the equilibrium capacity. Second, because of the slow increase in pressure the initial adsorption rate might be limited by the supply of CO_2 and thereby no truly intrinsic kinetics are measured. Because tuning of the PI control settings of the pressure control valve did not speed up the pressure increase sufficiently a bypass valve (V-2, Fig. 1) is installed. The pressure control valve (PCV-1, Fig. 1) and the bypass are opened in parallel. The bypass valve is closed after several hundreds of milliseconds depending on the desired reactor pressure. As shown in Fig. 6B the reactor pressure is significantly faster increased when V-2 is used. Thereby, CO_2 supply limitations are eliminated.

3.3. CO_2 concentration

External mass transfer limitations can be removed by using pure CO_2 as this will remove the film layer resistance. The effect of the CO_2 concentration is clearly seen in Fig. 7. The difference between 25% and 50% of CO_2 is a result of the increase in driving force for mass transfer with increasing concentration. Internally, mass transfer limitations by molecular diffusion will be eliminated by using pure CO_2. However, internal mass transfer limitations by Knudsen diffusion and viscous flow [47] might still influence the adsorption rate.

3.4. Particle size

The diameter of adsorbent particles will influence both, the internal and external heat and mass transfer properties. Where internal transfer is directly influenced by the diameter of the particle because of the penetration depth, external transfer is indirectly influenced since external heat and mass transfer coefficients are dependent on the diameter of the particle [51]. The diameter of the particles have been varied to see if heat and mass transfer limitations are minimized. In Fig. 8 is shown that largest fraction (355–500 µm) has a significant

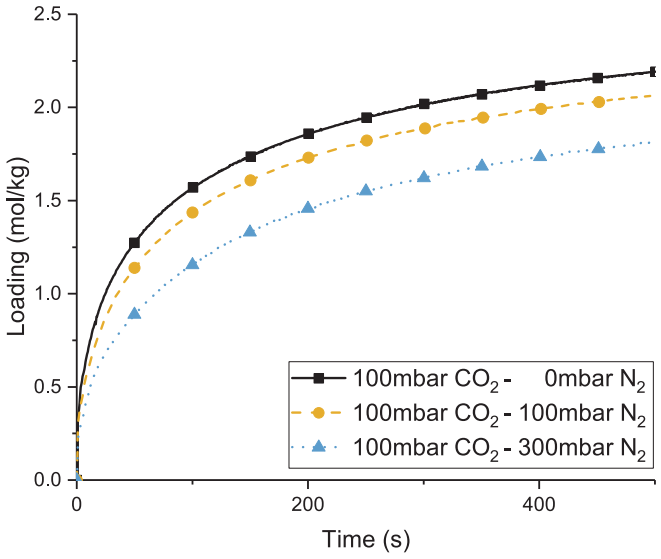

Fig. 7. Influence of the CO_2 concentration on reaction rate at 20 °C, 100 mbar of CO_2 pressure and particle diameter between 150 and 250 µm. Dilution of the CO_2 is performed by filling the reactor with nitrogen pressure (0/100/300 mbar N_2) before the start of the experiment. Symbols are added to increase distinction between lines.

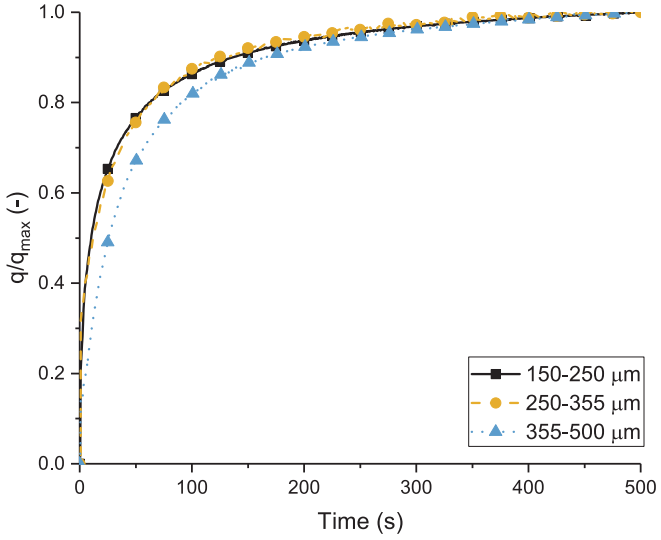

Fig. 8. Reaction rate as a function of sorbent particle size at 40 °C and 100 mbar of pure CO_2. Symbols are added to increase distinction between lines.

lower adsorption rate than the other two fractions. The adsorption rate for the 150–250 µm and 250–355 µm fractions are almost equal. The results found are in line with results published by Goeppert et al. [52] which showed that adsorption kinetics increase with smaller particle diameters. Additionally, Goeppert et al. showed that below 250 µm influence of particle diameter on adsorption rate is minimized, although Goeppert et al. used a PEI-based sorbent. The results in Fig. 8 show that by reducing the particle diameter the influence of mass and heat transfer is minimized. As the influence of external mass transfer is already excluded by using pure CO_2, heat transfer is most probably the reason that (355–500 µm) fraction has a lower adsorption rate. When the heat removal rate is not sufficient the particle temperature might increase and the equilibrium capacity might be influenced and with this the uptake rate. Next to that, to determine temperature dependency on kinetic parameters isothermal conditions are desirable. The influence of heat transfer and mass transfer inside the particles on the adsorption rate will be further discussed in relation to the particle model later on.

3.5. Summary

In the section above the influence of heat and mass transfer on the adsorption rate has been evaluated. Supply rate limitations of CO_2 have been eliminated by the use of a bypass valve. By using pure CO_2 limitations by external mass transfer and molecular diffusion into the sorbent pores have been removed. Analysis of the particle diameter showed that influence of heat transfer and internal mass transfer is minimized. All experiments discussed in Section 4 are performed with the particle diameter fraction between 150 and 250 µm.

4. Results and discussion

4.1. Effect of temperature and CO_2 pressure

The effect of temperature and pressure is shown in Fig. 9. It is clear that a higher pressure will lead to a higher adsorption rate as shown in Fig. 9B. The exact order of the reaction in the gas phase is discussed in the Section 4.2 below. A higher temperature will also increase the reaction rate as can be seen in Fig. 9A. The temperature dependency of the reaction rate will be described using the Arrhenius equation and is further discussed in Section 4.3.3.

In Fig. 9A is seen that loading for the 40 °C experiment levels off because it reaches the equilibrium capacity. The 40 °C experiment reaches the equilibrium capacity faster than the lower temperatures because of two reasons. First, the equilibrium capacity decreases with temperature, see Fig. 4. Second, because of the increased reaction rate the equilibrium capacities is reached quicker. Similarly to literature [26,27,29] it seen that the initial adsorption rate is high since it takes about 200 s to reach 80% of the equilibrium capacity. However, the last 20% takes over 1000 s at 40 °C. At 5 °C the situation is even worse; in the first 200 s about 50% of the equilibrium capacity is reached. However, reaching equilibrium at these low temperatures takes over an hour. This effect of temperature is of importance for air capture applications as the air capture system may behave totally different on a cold winter day compared to a hot summer day. Therefore, it is important to include temperature effects during design of the capture equipment.

4.2. Gas phase reaction order

In literature [12] it is shown that the reaction rate of CO_2 is first order in the gas phase concentration. This statement is verified by plotting the logarithm of the $\partial q/\partial t$ versus the CO_2 pressure in Fig. 10. The slope of the line is equal to power of the CO_2 pressure and thus the reaction order in the gas phase. $\partial q/\partial t$ is determined by fitting a rational polynomial – both first order in the nominator and denominator – to the loading versus time curve. Next, the derivative of the continuous polynomial can be determined. The reaction order in CO_2 partial pressure has been evaluated with experiments performed at 5 °C. Due to the slow reaction rate at 5 °C the reaction order can be evaluated at low loading and thereby the influence of equilibrium is minimized. In Fig. 10 can be seen that the apparent gas phase reaction order is an function of the loading. However, since the fits of 0.8 and 1.2 mol kg^{-1} are more accurate and the found reaction order is close to one it is concluded that the reaction order in the gas phase is indeed first order.

4.3. Reaction rate equation

The reaction rate equations presented in Section 2.4 are fitted to the experimental data to find the corrosponding kinetic rate constant. Experiments have been performed in the temperature range of 5–40 °C, at 50, 100 and 200 mbar of CO_2 pressure and using the particle diameter fraction between 150 and 250 µm. The fitting of k_{ads} is performed on the time range from 5 to 90 s. The starting point of 5 s is chosen to be sure that the pressure and temperature inside the reactor are constant in the

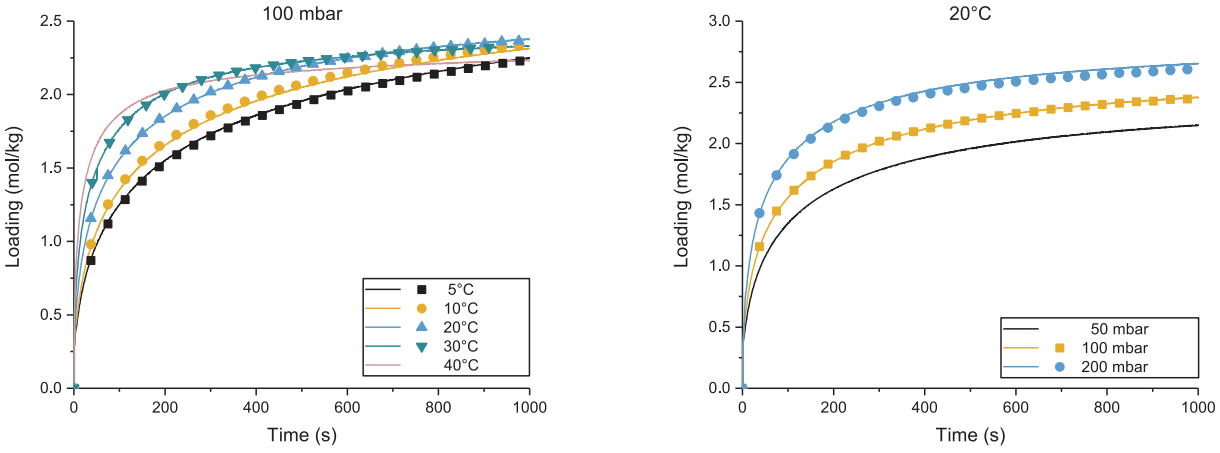

(A) Effect of temperature at 100mbar of CO_2 (B) Effect of CO_2 pressure at 20°C.

Fig. 9. Effect of temperature and pressure on the reaction rate for particle diameter between 150 and 250 µm. Lines show an experiment and symbols show a duplicate experiment.

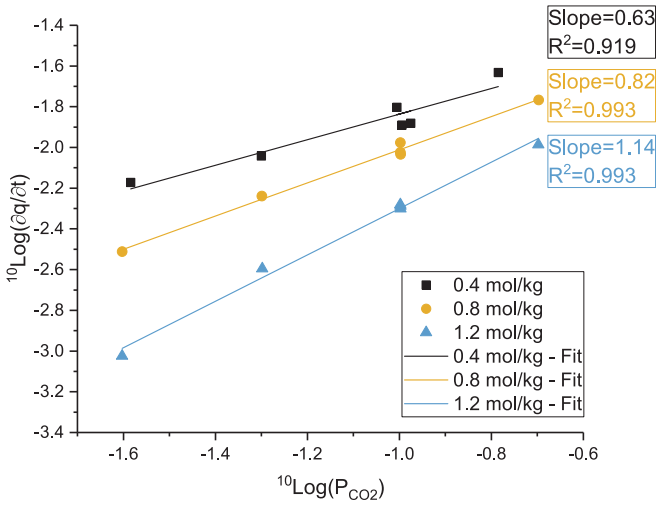

Fig. 10. Log–Log Plot to determine the reaction order in the gas phase. Experiments at 5 °C are used to fit at a low loading to minimize the influence of the equilibrium. Symbols represent the experimental point and lines show the linear fit.

fitting range. The end point 90 s is determined by minimizing the SSE (see Eq. 6) of the fit for the Toth isotherm with the Veneman parameters for varying time ranges. More details can be found in Section 3.1 of the Supporting Information. For every reaction rate equation the fit for a 100 mbar and 20 °C experiment is shown as an example. Moreover, the Arrhenius plot is given to see the temperature effect on the reaction rate parameters.

4.3.1. Linear driving force

First, the pseudo-first order linear driving force (PFO-LDF) and pseudo-second order linear driving force (PSO-LDF) rate equations are analysed. In Fig. 11 the results for the PFO-LDF rate equation are shown and in Fig. 12 the results of the PSO-LDF rate equation are shown. In Fig. 11A it seen that the pseudo-first order is not able to describe the shape of the experimental curve. In Section 3.2 of the Supporting Information the kinetic rate constant and SSE of all experiments fitted are reported. It is seen that the SSE is increasing with temperature and pressure. This shows that the steeper the loading curve versus time is, the worse the fit becomes. It can be concluded that the PFO-LDF is not a suitable equation to describe the adsorption reaction.

From the SSE in Fig. 12B can be seen that the PSO-LDF describes the shape of the experimental curve significantly better as the SSE is only one-third of the SSE of the PFO-LDF. The pseudo-second order fits better due to the second order in the number of free adsorption site. This accounts for the mechanism of adsorption in which two amine groups are needed to react with one CO_2 molecule in absence of H_2O. For the PSO-LDF no effects of temperature and pressure on the goodness-of-fit parameters were observed, see Section 3.1 of the Supporting Information. From Figs. 11B and 12B can be seen that the Arrhenius equation describes the temperature dependency well for the LDF equations. However, the influence of pressure is not accounted for correctly by the LDF models.

4.3.2. Toth rate equation

Second, the Toth reaction rate equation is evaluated with both parameters set A and B from Table 4. The results are given in Figs. 13 and 14. Overall is seen (Fig. 13A and 14A) that the fit of both Toth reaction rate equations are much better than the LDF equations. Evaluating the SSE of all experiments as shown in Section 3.2 of the Supporting Information shows that SSE for the Veneman et al. parameters (set A) is slightly higher than for the parameters presented in this work (set B). On the other hand, looking at the SSE of the Arrhenius plot in Figs. 13B and 14B shows the opposite. The Arrhenius fit has a lower SSE with the Veneman et al. parameters compared to the parameters from this work. Also remarkable is the difference in pre-exponential factor by a factor 1000. This might be an effect of the change in activation energy which is discussed in more detail below. It is important to emphasize the huge influence of the isotherm parameters on the kinetic constants found. Therefore, it is important to pay attention to both the isotherm parameters and the kinetic constants during fitting of the reaction rates.

4.3.3. Activation energy

Looking at the activation energy for the Veneman Toth fit E_{act} = 28.8 kJ mol^{-1} it seen that this is very close to the values found by Mukherjee et al. [19] for aqueous benzylamine reaction with CO_2 of 26 kJ mol^{-1}. Additionally, Wang et al. [36] found an activation energy in the same range of 31.7 kJ mol^{-1} for quaternary ammonium based resin of PES. On the other hand the activation energy of the PSO-LDF of 38.1 kJ mol^{-1} is similar to values reported by Richner et al. [20] (38 kJ mol^{-1}) and Penny and Ritter [53] (39.5 kJ mol^{-1}) for aqueous

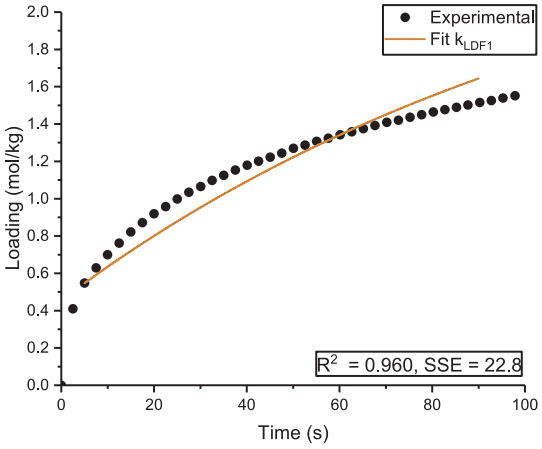

(A) Fit at 100mbar and 20°C.

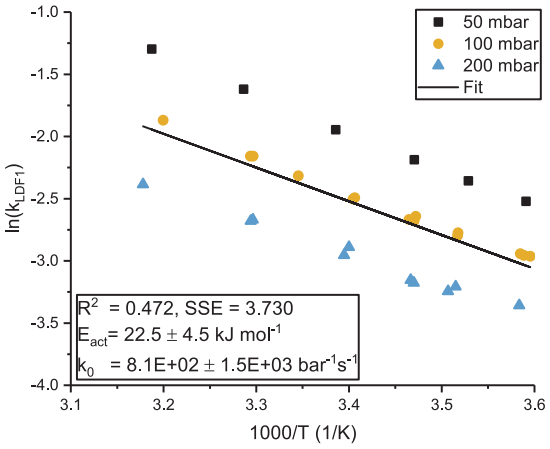

(B) Arrhenius plot

Fig. 11. Fit result and Arrhenius plot for pseudo-first order linear driving force (PFO-LDF) equation. The equilibrium capacity is determined by the isotherm from this work (set B).

benzylamine systems.

The activation energy (15.2 kJ mol^{-1}) of the Toth equation with the isotherm parameters from this work seems to be on the low side for a chemisorption system. Although, similar low values are reported in literature for other solid amine systems. Monazam et al. [54] reported a value of 13 kJ mol^{-1} for a amine/bentonite sorbent and Raja Shahrom et al. [55] found a value of 7.23 kJ mol^{-1} for a poly[VBTMA][Arg] sorbent.

The difference in activation energy for both the Toth rate equation fits might be explained by the equilibrium parameter *b*. The equilibrium parameter *b* is an Arrhenius type of equation with the isosteric heat of adsorption ΔH as parameter, see Table 2. The value of isosteric heat of adsorption will influence the temperature effect on the reverse reaction, see Eq. (5). As the degree of sorbent saturation in the fitting period (12–80%) is such that the reverse reaction can not be neglected, it might have an effect on the apparent temperature dependency of the forward reaction and consequently on the activation energy found.

4.3.4. *Verification of rate expression*

The found rate expressions are verified by use of the mathematical model presented in Section 2.6. In Fig. 15 it seen that the Toth rate equation with this works isotherm (set B) predicts the experiment better. However, it is seen that the deviation of the Veneman parameters (set A) is the effect of the error in prediction of the equilibrium capacity since the initial rate is correctly predicted. This is confirmed when looking at the SSE of all experiments in Section 3.3 of the Supporting Information. When fitting to 100 s no clear distinction can be made between the two isotherm sets. This shows that initial reaction rate is predicted correctly for both isotherm sets. However, looking at the SSE for the fit until 1000 s a clear effect of prediction of the equilibrium capacity is seen. For temperatures below 25 °C the isotherm from this work (set B) predicts the experiments better. However, inline with the parity plots presented in Fig. 5, the Veneman et al. isotherm (set A) predicts the experiments better at higher temperatures. In consequence, for longer times the isotherm parameters predicting equilibrium capacity are more important than the kinetic parameters for a good fit of experimental data.

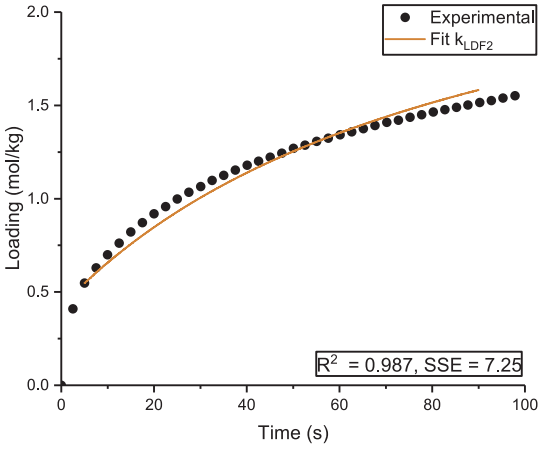

(A) Fit at 100mbar and 20°C.

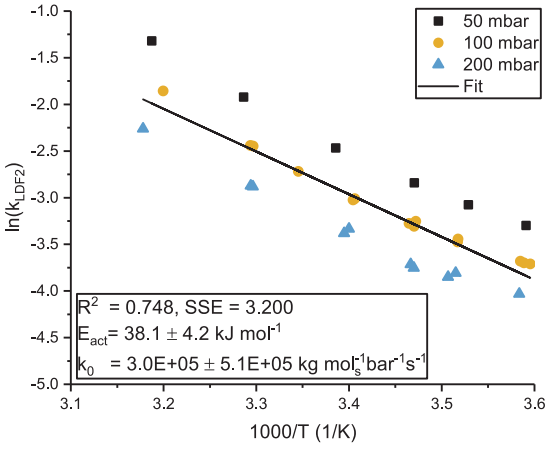

(B) Arrhenius plot

Fig. 12. Fit result and Arrhenius plot for pseudo-second order linear driving force (PSO-LDF) equation. The equilibrium capacity is determined by the isotherm from this work (set B).

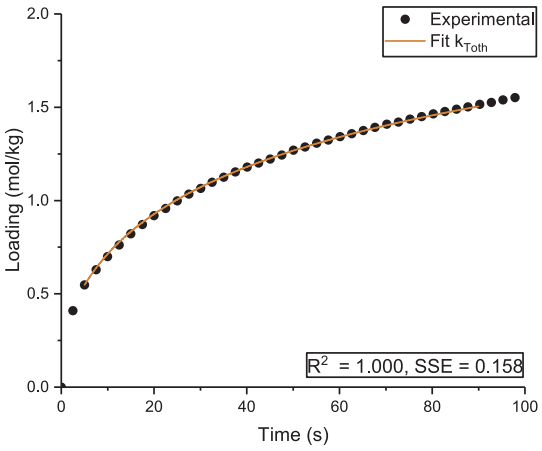

(A) Fit at 100mbar and 20°C.

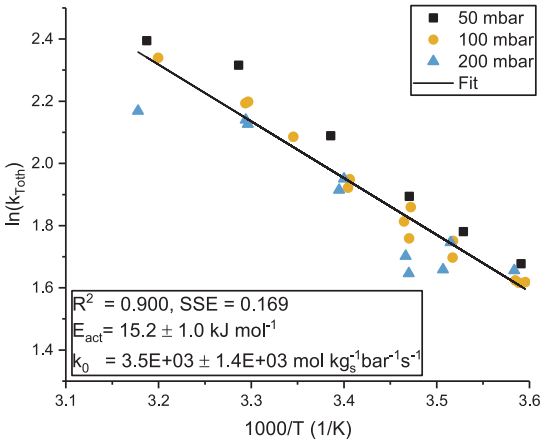

(B) Arrhenius plot

Fig. 13. Fit result and Arrhenius plot for Toth reaction rate equation using isotherm set B, this work.

4.3.5. Summary

The analysis above showed that the pseudo-first order LDF equation is not able to fit the data. The pseudo-second order LDF fits the temperature dependency of the adsorption rate. However, the pressure influence is not correctly described.

The Toth reaction rate equation describes both the temperature and pressure dependencies. The goodness-of-fit parameters for both sets of isotherm parameters (A & B, Table 4) are close. The quality of prediction of the initial reaction rate is independent of the isotherm and kinetic parameters. For longer times, however, the prediction of loading is strongly dependent on the prediction of the equilibrium capacity by the isotherm parameters used.

4.4. Experimental method verification

The particle model is used to verify that indeed intrinsic kinetics are measured and that heat and mass transfer limitations have been eliminated. The model presented in Section 2.6 has been used with the rate equation of Toth using the Veneman isotherm parameters. A worst case scenario for external heat transfer is assumed by using Nu = 2 for a stagnant gas around at particle. However, in the experiment most of the particles are in contact with the thermostated bottom of the reactor, which improves heat transfer by conduction.

In Fig. 16 the maximum temperature increase in the particle centre is shown for a fast, mediocre and slow experiment. It seen that the maximum temperature increase is about 8 K for the fastest experiment performed. However, at the start of the fitting interval at 5 s the temperature is almost back to the initial temperature. This shows that the effect of the temperature increase on the fit will be minimal. Especially, because the effects are smaller for the slower experiments and heat transfer is expected to be under predicted by the model.

Additionally, the radial profiles for the fastest experiment are studied in Fig. 17. In Fig. 17 can be seen that there is no radial temperature profile in the particle. This shows that heat transfer is externally limited, which might be an effect of the assumption of Nu = 2. However, as discussed before the external heat transfer might be larger in the experimental setup. Consequently, with increased external heat transfer the maximum temperature increase will be lower.

The concentration profile in Fig. 18 shows that in the first second a significant radial concentration profile is present. However, after 5 s the concentration inside the particle is almost equal to the bulk concentration. Therefore, it is not expected that the diffusional resistance

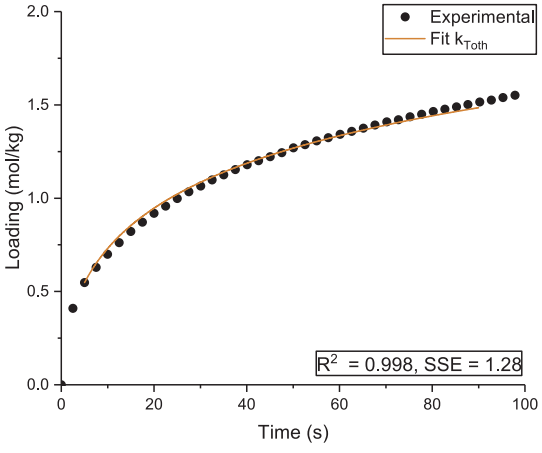

(A) Fit at 100mbar and 20°C.

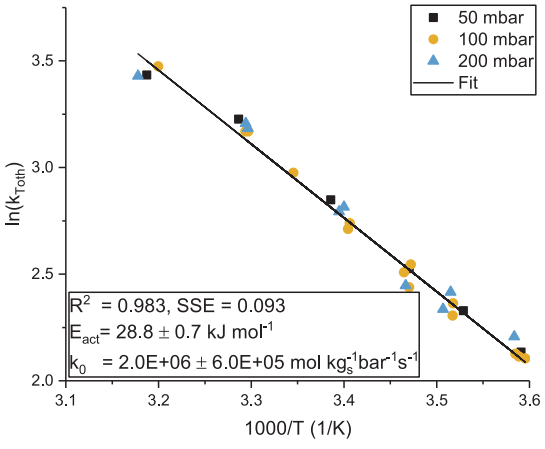

(B) Arrhenius plot

Fig. 14. Fit result and Arrhenius plot for Toth reaction rate equation using isotherm set A, Veneman et al. [49].

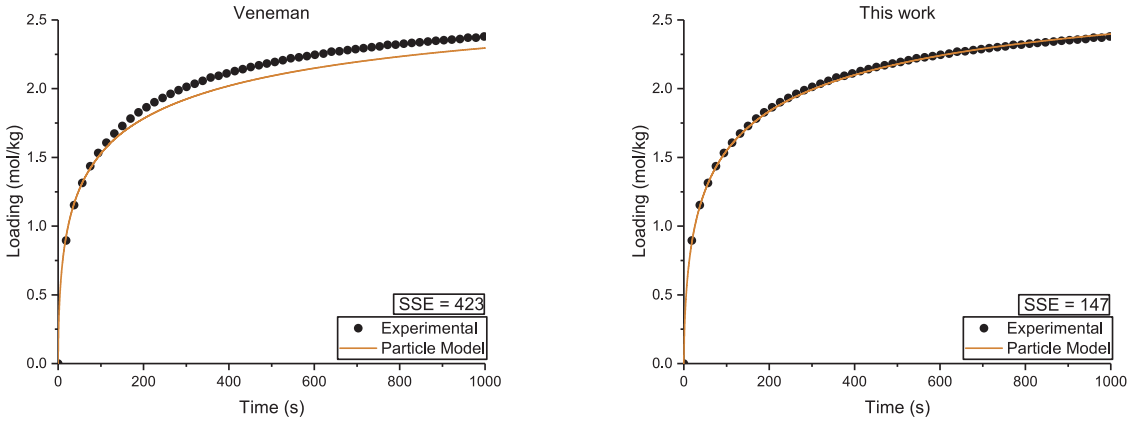

(A) Toth rate equation with Veneman et al isotherm parameters (set A).

(B) Toth rate equation with this work isotherm parameters (set B).

Fig. 15. Experimental loading and loading predicted by the model from Section 2.6 for a 100 mbar and 20 °C experiment.

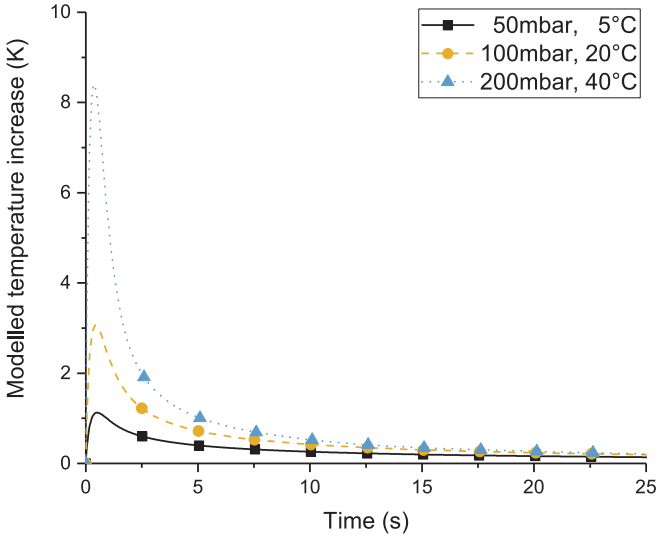

Fig. 16. Maximum temperature increase in particle centre for a fast, mediocre and slow experiment. Symbols are added to increase distinction between lines.

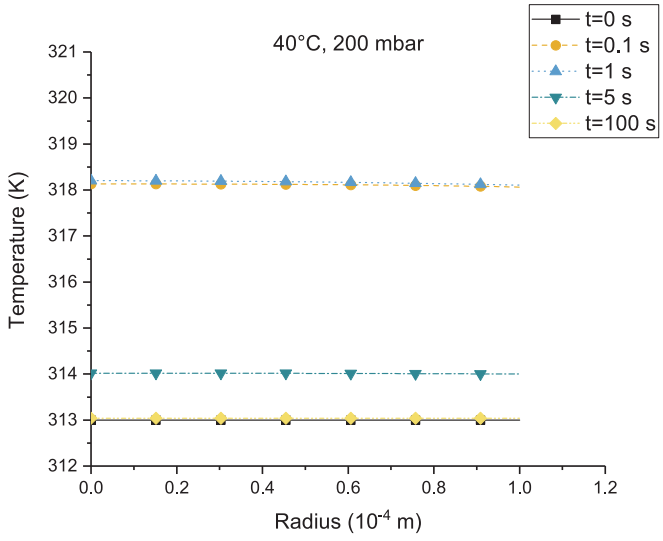

Fig. 17. The radial temperature profile inside the particle for a fast experiment at 200 mbar and 40 °C. Symbols are added to increase distinction between lines.

will influence fit results.

The above results from the particle model confirms that intrinsic kinetics are measured in this study. The influence of the initial mass and heat transfer limitations on the reaction rate are clearly negligible.

5. Conclusion

To measure the intrinsic reaction kinetics for CO2 adsorption on a solid amine sorbent an experimental method has been developed and applied. To ensure the absence of transport limitations, the influences of supply rate, heat and mass transfer on the adsorption rate have been evaluated. Supply rate limitations of CO_2 have been eliminated by the use of a bypass valve. By using pure CO_2 external mass transfer and molecular diffusion into the sorbent pores have been removed. Experimental analysis of the particle diameter showed that influence of heat transfer and internal mass transfer is minimal and mathematical modelling of the convection, diffusion and reaction rate inside the particle confirmed the absence of mass and heat transfer limitations and, hence, confirmed the measurement of intrinsic kinetics.

Analysis of the experimental data showed that the pseudo-first order and pseudo-second order linear driving force equations are not able to describe the experiments. Especially, the pseudo-first order linear driving force is not able to describe the strong non-linear behaviour of the particle loading in time. The Toth isotherm based rate equation was found to predict the experiments well. The found kinetic parameters show a strong correlation with the isotherm parameters used, especially for partially loaded sorbents. The above results show that for prediction of both the intial and equilibrium loading a rate based isotherm equation is necessary for consistent description of both kinetics and equilibrium.

Acknowledgement

The authors thank Benno Knaken, Johan Agterhorst and Karst van Bree for the construction of the setup and their technical support during the experimental phase.

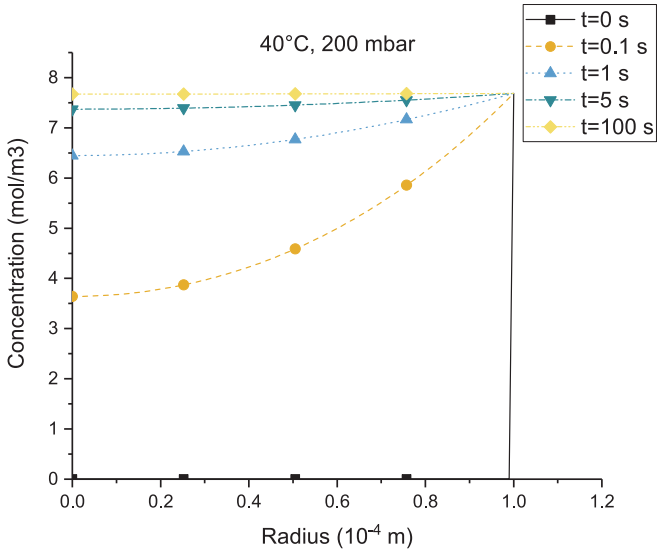

Fig. 18. The radial concentration profile inside the particle for a fast experiment at 200 mbar and 40 °C. Symbols are added to increase distinction between lines.

Appendix A. Supplementary data

Supplementary data associated with this article can be found, in the online version, athttps://doi.org/10.1016/j.cej.2018.11.072.

References

[1] B. Metz, O. Davidson, H. de Coninck, M. Loos, L. Meyer, IPCC special report on carbon dioxide capture and storage, Tech. Rep. (2005), https://doi.org/10.1002/anie.201000431.

[2] K.S. Lackner, S. Brennan, J.M. Matter, A.-H.A. Park, A. Wright, B. van der Zwaan, The urgency of the development of CO_2 capture from ambient air, Proc. Nat. Acad. Sci. 109 (33) (2012) 13156 LP – 13162.http://www.pnas.org/content/109/33/13156.abstract.

[3] P. Williamson, Emissions reduction: scrutinize CO2 removal methods, Nature 530 (7589) (2016) 153–155, https://doi.org/10.1038/530153a arXiv:arXiv:1011.1669v3,http://www.nature.com/doifinder/10.1038/530153a.

[4] IPCC, Climate Change 2014: Synthesis Report., Tech. rep., 2014.

[5] M.J. Bos, D.W.F. Brilman, A novel condensation reactor for efficient CO_2 to methanol conversion for storage of renewable electric energy, Chem. Eng. J. 278 (2015) 527–532, https://doi.org/10.1016/j.cej.2014.10.059.

[6] J.A. Martens, A. Bogaerts, N. De Kimpe, P.A. Jacobs, G.B. Marin, K. Rabaey, M. Saeys, S. Verhelst, The chemical route to a carbon dioxide neutral world, ChemSusChem 10 (6) (2017) 1039–1055, https://doi.org/10.1002/cssc.201601051.

[7] A. Goeppert, M. Czaun, J.-P. Jones, G.K. Surya Prakash, G.A. Olah, Recycling of carbon dioxide to methanol and derived products – closing the loop, Chem. Soc. Rev. 43 (23) (2014) 7995–8048, https://doi.org/10.1039/C4CS00122B URLhttp://xlink.rsc.org/?DOI=C4CS00122B.

[8] W. Brilman, L. Garcia Alba, R. Veneman, Capturing atmospheric CO_2 using supported amine sorbents for microalgae cultivation, Biomass Bioenergy 53 (2013) 39–47, https://doi.org/10.1016/j.biombioe.2013.02.042.

[9] S. Choi, J.H. Drese, C.W. Jones, Adsorbent materials for carbon dioxide capture from large anthropogenic point sources, ChemSusChem 2 (9) (2009) 796–854, https://doi.org/10.1002/cssc.200900036.

[10] F. Shakerian, K.H. Kim, J.E. Szulejko, J.W. Park, A comparative review between amines and ammonia as sorptive media for post-combustion CO_2 capture, Appl. Energy 148 (2015) 10–22, https://doi.org/10.1016/j.apenergy.2015.03.026 arXiv:arXiv:1011.1669v3.

[11] E.E. Ünveren, B. ÖMonkul, E. Sarolan, N. Karademir, E. Alper, Solid amine sorbents for CO_2 capture by chemical adsorption: a review, Petroleum 3 (1) (2017) 37–50, https://doi.org/10.1016/j.petlm.2016.11.001.

[12] R. Veneman, T. Hilbers, D.W.F. Brilman, S.R.A. Kersten, CO2 capture in a continuous gas-solid trickle flow reactor, Chem. Eng. J. 289 (2016) 191–202, https://doi.org/10.1016/j.cej.2015.12.066.

[13] S. Sutanto, J.W. Dijkstra, J.A.Z. Pieterse, J. Boon, P. Hauwert, D.W.F. Brilman, CO2 removal from biogas with supported amine sorbents: first technical evaluation based on experimental data, Sep. Purif. Technol. 184 (2017) 12–25, https://doi.org/10.1016/j.seppur.2017.04.030 URLhttp://www.sciencedirect.com/science/article/pii/S138358661731256X.

[14] E. Sonnleitner, G. Schöny, H. Hofbauer, Assessment of zeolite 13X and Lewatit VP OC 1065 for application in a continuous temperature swing adsorption process for biogas upgrading, Biomass Conversion Biorefineryhttps://doi.org/10.1007/s13399-017-0293-3.http://link.springer.com/10.1007/s13399-017-0293-3.

[15] R.T. Driessen, M.J. Bos, D.W. Brilman, A multistage fluidized bed for the deep removal of sour gases: proof of concept and tray efficiencies, Ind. Eng. Chem. Res. 57 (11) (2018) 3866–3875, https://doi.org/10.1021/acs.iecr.7b04891 URLhttp://pubs.acs.org/doi/10.1021/acs.iecr.7b04891.

[16] Q. Yu, D.W.F. Brilman, Design strategy for CO_2 adsorption from ambient air using a supported amine based sorbent in a fixed bed reactor, Energy Procedia 114 (2017) 6102–6114, https://doi.org/10.1016/j.egypro.2017.03.1747 URLhttp://www.sciencedirect.com/science/article/pii/S1876610217319495.

[17] M. Caplow, Kinetics of carbamate formation and breakdown, J. Am. Chem. Soc. 90 (24) (1968) 6795–6803, https://doi.org/10.1021/ja01026a041.

[18] J.E. Crooks, J.P. Donnellan, Kinetics and mechanism of the reaction between carbon dioxide and amines in aqueous solution, J. Chem. Soc. Perkin Trans. 2 (4) (1989) 331–333, https://doi.org/10.1039/P29890000331.

[19] S. Mukherjee, S.S. Bandyopadhyay, A.N. Samanta, Kinetic study of CO_2 absorption in aqueous benzylamine solvent using a stirred cell reaction calorimeter, Energy Fuels (2018), https://doi.org/10.1021/acs.energyfuels.7b03743 acs.energyfuels.7b03743.

[20] G. Richner, G. Puxty, A. Carnal, W. Conway, M. Maeder, P. Pearson, Thermokinetic properties and performance evaluation of benzylamine-based solvents for CO2capture, Chem. Eng. J. 264 (2015) 230–240, https://doi.org/10.1016/j.cej.2014.11.067.

[21] W. Buijs, S. de Flart, Direct air capture of CO_2 with an amine resin: a molecular modeling study of the CO_2 capturing process, Ind. Eng. Chem. Res. 56 (43) (2017) 12297–12304, https://doi.org/10.1021/acs.iecr.7b02613 URLhttp://pubs.acs.org/doi/abs/10.1021/acs.iecr.7b02613.

[22] D.S. Mebane, J.D. Kress, C.B. Storlie, D.J. Fauth, M.L. Gray, K. Li, Transport, zwitterions, and the role of water for CO_2 adsorption in mesoporous silica-supported amine sorbents, J. Phys. Chem. C 117 (50) (2013) 26617–26627, https://doi.org/10.1021/jp4076417.

[23] M.W. Hahn, M. Steib, A. Jentys, J.A. Lercher, Mechanism and kinetics of CO_2 adsorption on surface bonded amines, J. Phys. Chem. C 119 (8) (2015) 4126–4135, https://doi.org/10.1021/jp512001t.

[24] J. Yu, S.S. Chuang, The structure of adsorbed species on immobilized amines in CO2 capture: an in situ IR study, Energy Fuels 30 (9) (2016) 7579–7587, https://doi.org/10.1021/acs.energyfuels.6b01423.

[25] Z. Bacsik, N. Ahlsten, A. Ziadi, G. Zhao, A.E. Garcia-Bennett, B. Martín-Matute, N. Hedin, Mechanisms and kinetics for sorption of CO_2 on bicontinuous mesoporous silica modified with n-propylamine, Langmuir 27 (17) (2011) 11118–11128, https://doi.org/10.1021/la202033p.

[26] P. Bollini, N.A. Brunelli, S.A. Didas, C.W. Jones, Dynamics of CO_2 adsorption on amine adsorbents. 2. Insights into adsorbent design, Ind. Eng. Chem. Res. 51 (46) (2012) 15153–15162, https://doi.org/10.1021/ie3017913.

[27] W. Jung, J. Park, K.S. Lee, Kinetic modeling of CO_2 adsorption on an amine-functionalized solid sorbent, Chem. Eng. Sci. 177 (2018) 122–131, https://doi.org/10.1016/j.ces.2017.11.003.

[28] Q. Liu, J. Shi, S. Zheng, M. Tao, Y. He, Y. Shi, L.P. S, Kinetics Studies of CO_2 Adsorption/Desorption on Amine- functionalized Multi-walled Carbon Nanotubes (2014) 1–9.

[29] R. Serna-Guerrero, A. Sayari, Modeling adsorption of CO_2 on amine-functionalized mesoporous silica. 2: Kinetics and breakthrough curves, Chem. Eng. J. 161 (1–2) (2010) 182–190, https://doi.org/10.1016/j.cej.2010.04.042.

[30] A. Abdollahi Govar, A.D. Ebner, J.A. Ritter, Effect of H_2O vapor on the adsorption and desorption behavior of CO_2 in a solid amine sorbent, Energy Fuels (2016), https://doi.org/10.1021/acs.energyfuels.6b01797 acs.energyfuels.6b01797.

[31] A.D. Ebner, S.P. Reynolds, J.A. Ritter, Nonequilibrium kinetic model that describes the reversible adsorption and desorption behavior of CO_2 in a K-promoted hydrotalcite-like compound, Ind. Eng. Chem. Res. 46 (6) (2007) 1737–1744, https://doi.org/10.1021/ie061042k.

[32] N.A. Rashidi, S. Yusup, B.H. Hameed, Kinetic studies on carbon dioxide capture using lignocellulosic based activated carbon, Energy 61 (2013) 440–446, https://doi.org/10.1016/j.energy.2013.08.050.

[33] C. Goel, H. Kaur, H. Bhunia, P.K. Bajpai, Carbon dioxide adsorption on nitrogen enriched carbon adsorbents: Experimental kinetics isothermal and thermodynamic studies, J. CO_2 Util. 16 (2016) 50–63, https://doi.org/10.1016/j.jcou.2016.06.002.

[34] E.R. Monazam, L.J. Shadle, R. Siriwardane, Equilibrium and absorption kinetics of carbon dioxide by solid supported amine sorbent, AIChE J. 57 (11) (2011) 3153–3159, https://doi.org/10.1002/aic.12516.

[35] A. Zhao, A. Samanta, P. Sarkar, R. Gupta, Carbon dioxide adsorption on amine-impregnated mesoporous SBA-15 sorbents: experimental and kinetics study, Ind. Eng. Chem. Res. 52 (19) (2013) 6480–6491, https://doi.org/10.1021/ie3030533.

[36] T. Wang, J. Liu, H. Huang, M. Fang, Z. Luo, Preparation and kinetics of a heterogeneous sorbent for CO_2 capture from the atmosphere, Chem. Eng. J. 284 (2016) 679–686, https://doi.org/10.1016/j.cej.2015.09.009 URLhttp://www.sciencedirect.com/science/article/pii/S1385894715012632?via=ihub.

[37] X. Hu, S. Brandani, A.I. Benin, R.R. Willis, Development of a semiautomated zero length column technique for carbon capture applications: study of diffusion behavior of CO_2 in MOFs, Ind. Eng. Chem. Res. 54 (21) (2015) 5777–5783, https://doi.org/10.1021/acs.iecr.5b00515.

[38] W.R. Alesi, J.R. Kitchin, Evaluation of a primary amine-functionalized ion-exchange resin for CO_2 capture, Ind. Eng. Chem. Res. 51 (19) (2012) 6907–6915, https://doi.org/10.1021/ie300452c.

[39] Lanxess, Lewatit VP OC 1065 Technical Data Sheet, Tech. rep., 2016.

[40] P. Linstrom, W. Mallard, NIST Chemistry WebBook, NIST Standard Reference Database Number 69, National Institute of Standards and Technology, Gaithersburg

MD, 2018, https://doi.org/10.18434/T4D303.
[41] P.E. Liley, G.H. Thomson, D. Friend, T.E. Daubert, E. Buck, Physical and chemical data, in: M. Hill (Ed.), Perry's Chemical Engineers' Handbook, seventh ed., 1997, pp. 2–141.
[42] E. Glueckauf, J.I. Coates, 241. Theory of chromatography. Part IV. The influence of incomplete equilibrium on the front boundary of chromatograms and on the effectiveness of separation, J. Chem. Soc. (Resumed) 1315–1321 (1947), https://doi.org/10.1039/JR9470001315.
[43] S. Lagergren, About the theory of so-called adsorption of soluble substances, Kungliga Svenska Vetenskapsakademiens Handlingar 24 (4) (1898) 1–39.
[44] A.E. Rodrigues, C.M. Silva, What's wrong with Lagergreen pseudo first order model for adsorption kinetics? Chem. Eng. J. 306 (2016) 1138–1142, https://doi.org/10.1016/j.cej.2016.08.055.
[45] D.D. Do, Analysis of Adsorption Kinetics in a Single Homogeneous Particle, in: Adsorption Analysis: Equilibria and Kinetics, Vol. Volume 2 of Series on Chemical Engineering, Published by Imperial College Press and Distributed by World Scientific Publishing Co., 1998, pp. 519–602.https://doi.org/10.1142/9781860943829_0009.
[46] J.R. Taylor, An introduction to error analysis, University Science Books, Sausalito, Calif, 1997.
[47] D.D. Do, Fundamentals of Diffusion and Adsorption in Porous Media, in: Adsorption Analysis: Equilibria and Kinetics, Vol. Volume 2 of Series on Chemical Engineering, 1998, pp. 337–414.https://doi.org/10.1142/9781860943829_0007.
[48] P. Zehner, U.E. Schlünder, Wärmeleitfähigkeit von Schüttungen bei mäßigen Temperaturen, Chem. Ing. Tech. 42 (14) (1970) 933–941, https://doi.org/10.1002/cite.330421408.
[49] R. Veneman, N. Frigka, W. Zhao, Z. Li, S. Kersten, W. Brilman, Adsorption of H_2O and CO_2 on supported amine sorbents, Int. J. Greenhouse Gas Control 41 (2015) 268–275, https://doi.org/10.1016/j.ijggc.2015.07.014 URLhttp://linkinghub.elsevier.com/retrieve/pii/S1750583615300219.
[50] Q. Yu, J.D.L.P. Delgado, R. Veneman, D.W.F. Brilman, Stability of a benzyl amine based CO_2 capture adsorbent in view of regeneration strategies, Ind. Eng. Chem. Res. 56 (12) (2017) 3259–3269, https://doi.org/10.1021/acs.iecr.6b04645 URLhttp://pubs.acs.org/doi/abs/10.1021/acs.iecr.6b04645.
[51] R.B. Bird, W.E. Stewart, E.N. Lightfoot, Transport Phenomena, second ed., John Wiley & Sons Ltd, 2007.
[52] A. Goeppert, H. Zhang, M. Czaun, R.B. May, G.K. Prakash, G.A. Olah, S.R. Narayanan, Easily regenerable solid adsorbents based on polyamines for carbon dioxide capture from the air, ChemSusChem 7 (5) (2014) 1386–1397, https://doi.org/10.1002/cssc.201301114.
[53] D.E. Penny, T.J. Ritter, Kinetic study of the reaction between carbon dioxide and primary amines, J. Chem. Soc. Faraday Trans. 1: Phys. Chem. Condensed Phases 79 (9) (1983) 2103, https://doi.org/10.1039/f19837902103 URLhttp://xlink.rsc.org/?DOI=f19837902103.
[54] E.R. Monazam, L.J. Shadle, R. Siriwardane, Performance and kinetics of a solid amine sorbent for carbon dioxide removal, Ind. Eng. Chem. Res. 50 (19) (2011) 10989–10995, https://doi.org/10.1021/ie201214q.
[55] M.S. Raja Shahrom, C.D. Wilfred, F.K. Chong, Thermodynamic and kinetic studies on CO_2 capture with Poly[VBTMA][Arg], J. Phys. Chem. Solids 116 (2017) (2018) 22–29, https://doi.org/10.1016/j.jpcs.2018.01.008.